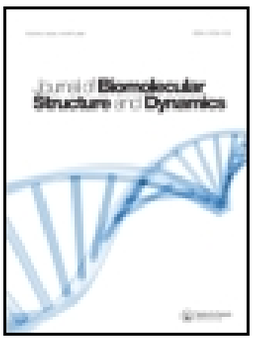

Taylor & Francis
Taylor & Francis Group

Journal of Biomolecular Structure and Dynamics

ISSN: 0739-1102 (Print) 1538-0254 (Online) Journal homepage: http://www.tandfonline.com/loi/tbsd20

Terahertz vibration modes in Na/K-ATPase

Alberto Carpinteri, Gianfranco Piana, Andrea Bassani & Giuseppe Lacidogna

To cite this article: Alberto Carpinteri, Gianfranco Piana, Andrea Bassani & Giuseppe Lacidogna (2018): Terahertz vibration modes in Na/K-ATPase, Journal of Biomolecular Structure and Dynamics, DOI: 10.1080/07391102.2018.1425638

To link to this article: https://doi.org/10.1080/07391102.2018.1425638

Accepted author version posted online: 08 Jan 2018.
Published online: 24 Jan 2018.

Journal of Biomolecular Structure and Dynamics, 2018
https://doi.org/10.1080/07391102.2018.1425638

Terahertz vibration modes in Na/K-ATPase

Alberto Carpinteri, Gianfranco Piana, Andrea Bassani and Giuseppe Lacidogna*

Department of Structural, Geotechnical and Building Engineering, Politecnico di Torino, Corso Duca degli Abruzzi 24, 10129, Torino, Italy

Communicated by Ramaswamy H. Sarma

(*Received 18 December 2017; accepted 4 January 2018*)

Mechanical vibration in the Terahertz range is believed to be connected with protein functions. In this paper, we present the results of a normal-mode analysis (modal analysis) of a Na/K-ATPase all-atom model, focusing the attention on low-frequency vibration modes. The numerical model helps in the interpretation of experimental results previously obtained by the authors via Raman spectroscopy of Na/K-ATPase samples, where several unassigned peaks were found in the sub-500 cm^{-1} range. In particular, vibration modes corresponding to peaks at 27, 190 and 300 cm^{-1}, found experimentally, are confirmed here numerically, together with some other modes at lower frequencies (wavenumbers) that were not possible to observe in the experimental test. All the aforementioned modes correspond to vibrations involving the protein ends, i.e. portions directly related to the operating mechanism of the sodium-potassium pump.

Keywords: sodium-potassium pump; THz vibration; all-atom simulation; modal analysis; lattice model

1. Introduction

Na+/K+-adenosine triphosphatase (Na/K-ATPase), also known as the sodium–potassium pump, is a membrane protein (enzyme) crucial in regulating cell homoeostasis. Although many membrane protein structures are already well determined, their functioning is still difficult to investigate because they are fully functional only in the *in vivo* membranous environment. Several specific methodologies were developed to investigate various aspects of their cellular life but they are still challenging for effective computational methods. Among other proteins, Na/K-ATPase, whose structure is well-known, is now recognized as an important therapeutic target for the treatment of several human diseases, from metabolic dysfunctions to neurodegenerative illnesses and cancer. Information on its vibrational behaviour are thus of interest because of the possibility to interfere with the biological structure by means of low-frequency electromagnetic waves resonating with the thermal fluctuations (Lucia, 2016; Lucia, Grisolia, Ponzetto, & Silvagno, 2017; Lucia & Ponzetto, 2017).

The directions of the largest thermal fluctuations of the structure of a protein in its native state are the directions of its low-frequency modes (below 1 THz), named acoustical modes by analogy with the acoustical phonons of a material. The acoustical modes of a protein assist its conformational changes and are related to its biological functions (Cui, Li, Ma, & Karplus, 2004; Gaillard, Dejaegere, & Stote, 2009). Since nearly four decades up to today, there has been a considerable interest in establishing the possible role of the low-frequency (<200 cm^{-1}) modes of proteins for their biological function (Bennett & Huber, 1984; Berendsen & Hayward, 2000; Gerstein & Krebs, 1998; Gerstein, Lesk, & Chothia, 1994; Hayward & Berendsen, 1998; Karplus & Petsko, 1990; McCammon, 1984; McCammon, Gelin, & Karplus, 1976; Rod, Radkiewicz, & Brooks, 2003; Tama & Sanejouand, 2001). To perform their functions, most of the proteins need to alternate between different states which are separated by activation barriers. The passage from one state to another is coupled to the binding/release of one or more ligands and could be assisted by confined acoustical modes (Berendsen & Hayward, 2000; Tama & Sanejouand, 2001; Tobi & Bahar, 2005). The directions of the low-frequency modes provide the directions of the largest deformations at thermal equilibrium and can serve as collective coordinates to describe the conformational changes (Hayward & Berendsen, 1998; Gerstein & Krebs, 1998; Gerstein et al., 1994). The low-frequency modes are related to the amino-acid sequence of the protein because they depend on the tertiary structure. Proteins for which the amino-acid sequences lead to the same fold (having the same main-chain conformation) have similar confined acoustical modes because the lowest frequency modes depend mainly on the connectivity of the main chain of the protein and not on the atomistic details. Natural selection of an amino-acid sequence not only selects a structure, and

*Corresponding author. Email: giuseppe.lacidogna@polito.it

thus a biological function, but also the low-frequency collective modes associated to it. Since low-frequency modes are still difficult to detect experimentally, computational models are thus of help in their identification (Liwo, 2013).

In this study, using the same approach that we adopted in a previous study about Lysozyme (Carpinteri, Lacidogna, Piana, & Bassani, 2017), we investigate the low-frequency vibration modes of Na/K-ATPase by a structural lattice model of the entire protein implemented in a finite element commercial code. On the one hand, the results of the simulation (natural frequencies and modes of vibration) are used to associate a mode shape to the low-frequency spectral peaks previously obtained experimentally by the authors through Raman spectroscopy measurements (Lacidogna, Piana, Bassani, & Carpinteri, 2017). In addition, the numerical results are also used to detect other vibration modes corresponding to frequencies lower than those that it was possible to detect experimentally.

2. Materials and methods

Na/K-ATPase is a quite large protein composed by 1028 amino acids (10,131 atoms). It has a Y-like three-dimensional structure, with an average diameter of about 4 nm and a length about 16 nm. Its molecular weight is equal to approximately 110 kDa (1.78×10^{-22} kg). A linear-elastic structural model of the entire protein was built, according to the following assumptions and methods, in order to investigate the small-amplitude vibrations of the protein crystal structure around its equilibrium configuration.

Under the assumption of small displacements with respect to the equilibrium distances, attractive/repulsive forces between atoms can be modelled, the precision increasing with the smallness of the displacement, by linear-elastic springs (Feynman, Leighton, & Sands, 1964). Bonds between atoms of the same kind are covalent, as well as bonds between atoms having similar electronegativities are also predominantly covalent. Despite covalent bond energies and lengths depend on several factors, it is a general rule that the shorter the bond length and the higher the bond energy and vice versa. The potential energy associated to a covalent bond is basically made of two parts: an attractive contribution and a repulsive one. This can be empirically expressed as (Pauling, 1960):

$$U(r) = -\frac{A}{r^m} + \frac{B}{r^n} \quad (\text{with } m < n,\ m > 2), \tag{1}$$

where A and B are positive constants (depending on the nature of interacting atoms), and r is the distance between atoms. The first and the second terms of the right-hand side of Equation (1) represent the attractive and the repulsive energy, respectively. The former prevails at large interatomic distances (large r), whereas the latter dominates at short distances (small r); note that the right-hand side of Equation (1) diverges for $r \to 0$. For intermediate distances, a balance between the two terms is expected, with the consequent presence of a minimum of the potential energy (Figure 1(a)). The equilibrium position (distance), r_0, is therefore defined by setting the first derivative of function $U(r)$ equal to zero (minimum of potential energy):

$$\frac{\mathrm{d}U}{\mathrm{d}r} = 0 \Leftrightarrow r = r_0. \tag{2}$$

The interatomic force, $F = -\mathrm{d}U/\mathrm{d}r$, is attractive for $r > r_0$ ($\mathrm{d}U/\mathrm{d}r > 0$), repulsive for $r < r_0$ ($\mathrm{d}U/\mathrm{d}r < 0$), and null for $r = r_0$ (Figure 1(a)). Other empirical expressions of the potential $U(r)$ can be adopted. For instance, the Morse potential has been specifically developed to describe the covalent bond between a couple of atoms (Morse, 1929). However, unlike that of Equation (1), the Morse potential does not diverge for $r \to 0$ and consequently it must be used for interatomic distances not much smaller than the equilibrium distance.

The study of the small-amplitude atomic oscillations around the equilibrium position requires considering the second-order Taylor series expansion of the potential (harmonic approximation):

$$U(r) \cong U(r_0) + \left(\frac{\mathrm{d}U}{\mathrm{d}r}\right)_{r=r_0} (r - r_0) + \frac{1}{2}\left(\frac{\mathrm{d}^2U}{\mathrm{d}r^2}\right)_{r=r_0} (r - r_0)^2. \tag{3}$$

Recalling Equation (2) and defining the force constant (stiffness) k as:

$$k := -\left(\frac{\mathrm{d}F}{\mathrm{d}r}\right)_{r=r_0} = \left(\frac{\mathrm{d}^2U}{\mathrm{d}r^2}\right)_{r=r_0}, \tag{4}$$

the harmonic approximation of the potential becomes (Figure 1(b)):

$$U(r) \cong U(r_0) + \frac{1}{2}k(r - r_0)^2. \tag{5}$$

Therefore, near r_0, we obtain the linear expression for the interatomic force (Figure 1(b)):

$$F = -k(r - r_0) = -kx, \tag{6}$$

where we have set $x = (r - r_0)$ the relative displacement. In this way, for example, the small-amplitude vibration of a diatomic molecule, modelled by two masses m_1 and m_2 connected by a linear-elastic spring of stiffness k, can be described by the well-known equation of the harmonic oscillator:

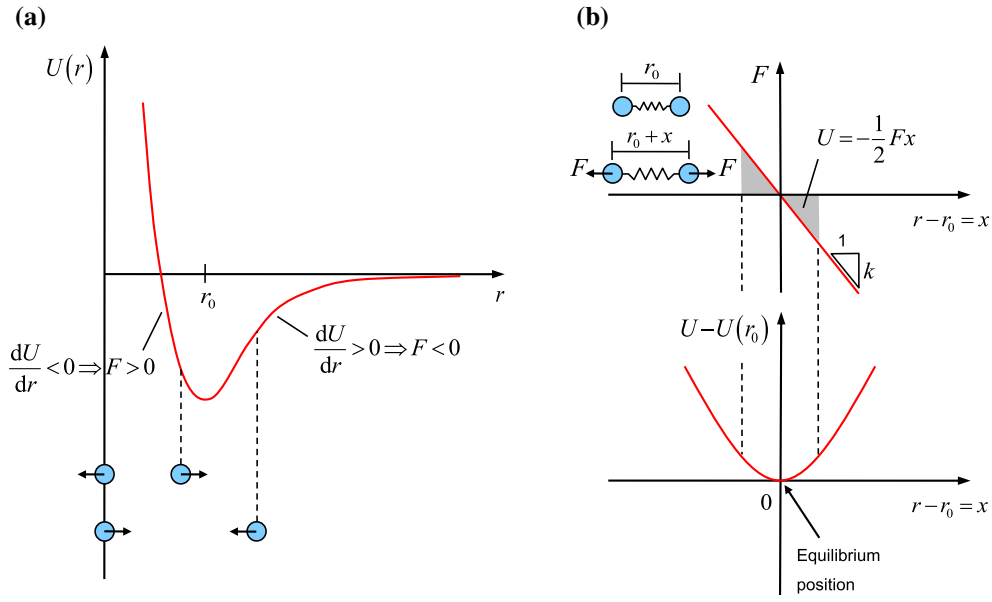

Figure 1. Model of interatomic bond: (a) potential energy versus interatomic distance; (b) harmonic approximation near the equilibrium distance (two atoms joined by a spring).

$$\mu \frac{\mathrm{d}^2 x}{\mathrm{d}t^2} + kx = 0, \tag{7}$$

where $x = x(t)$ is the relative displacement of the two masses, $\mu = m_1 m_2 / m_1 + m_2$ is the reduced mass, and t is time. The time solution of Equation (7) is cosinusoidal, with frequency of oscillation (natural frequency) $f = \sqrt{k/\mu}/2\pi$ ($\mathrm{s}^{-1} = \mathrm{Hz}$); angular frequency of oscillation $\omega = 2\pi f$ (rad s^{-1}) (Feynman et al., 1964).

An equation formally analogous to Equation (7) can be written in matrix form for a more complex assembly of point masses connected by elastic springs as (time derivative is indicated by a dot):

$$\underset{(N\times N)}{\mathbf{M}} \cdot \underset{(N\times 1)}{\ddot{\mathbf{x}}(t)} + \underset{(N\times N)}{\mathbf{K}} \cdot \underset{(N\times 1)}{\mathbf{x}(t)} = \underset{(N\times 1)}{\mathbf{0}}, \tag{8}$$

where $\mathbf{x}(t)$ is the displacement vector, depending on the generalized coordinates describing the motion, **M** and **K** are the mass and stiffness matrices, constant in time and depending on mass and elastic constant values, respectively; their structure is defined by the topology of the assembly; N is the number of degrees of freedom of the system. Equation (8) governs the undamped free dynamics of a generic mass-spring assembly with N degrees of freedom. Assuming a harmonic response in the form $\mathbf{x}(t) = \mathbf{x}_0 \mathbf{e}^{\mathbf{i}\omega t}$, one obtains the following homogeneous linear system of algebraic equations (generalized eigenproblem) (Clough & Penzien, 1975):

$$\left(\mathbf{K} - \omega^2 \mathbf{M}\right) \cdot \mathbf{x}_0 = 0, \tag{9}$$

the non-trivial solution of which gives eigenvectors, as well as the eigenvalues ω^2 (square of the natural angular frequencies of the system) by solving the algebraic equation of order N (characteristic equation) resulting from the following condition:

$$\det\left(\mathbf{K} - \omega^2 \mathbf{M}\right) = 0. \tag{10}$$

Once the eigenvalues have been determined, Equation (9) allows to obtain the eigenvectors $\mathbf{x}_0$ (vibration modes). A system with N degrees of freedom will therefore present N natural frequencies as well as N vibration modes.

A structural finite element model of the Na/N-ATPase crystal structure was built with the commercial code LUSAS (http://www.lusas.com) in order to solve the eigenproblem (9). The protein was modelled as a cloud of point-masses (atoms) interconnected by linear springs simulating interatomic bonds; only covalent bonds were considered, neglecting all weaker bonds. A lattice model was therefore obtained with masses concentrated at the nodes and bonds simulated by linear-elastic, massless beams. The beam ends were internally clamped at each node in order to avoid rotational labilities in the obtained lattice (bending and torsion relative rotations of the beam ends were prevented). Only the axial deformation of the beams was taken into account: this was achieved by providing each beam with bending and torsion rigidities much greater than axial rigidity, so as to inhibit both bending and torsion relative deformations; also, shear deformation was not included in the model. In general, the axial stiffness k_i of the i-th beam is expressed as (Carpinteri, 1997):

$$k_i = \frac{E_i A_i}{l_i}, \tag{11}$$

being E_i (FL^{-2}) the Young's modulus, A_i (L^2) and l_i (L) the cross-sectional area and the beam length, respectively. In the model, the values of $E_i = E$ and $A_i = A$ were set equal for all beams and chosen so as to reproduce the desired bond stiffness. Bending and (primary, St. Venant) torsion beam stiffnesses depend on length l_i, and on bending, EI_{ij}, and torsion, GJ_i, rigidities, respectively; I_{ij} (L^4) denotes the area moment of inertia of the cross-section with respect to the principal axis j ($j = 1, 2$); G (FL^{-2}) is the shear modulus ($G = E/2(1 + \nu)$, with ν (/) the Poisson's ratio); and J_i (L^4) denotes the St. Venant torsion constant (Carpinteri, 1997). Starting from beam lengths l_i and axial, bending, and torsion rigidities, the local (element) stiffness matrix $\mathbf{K_e}$ can be computed. On the other hand, knowing the point masses m_k ($k = 1, 2, ..., n$) allows to obtain also the local mass matrix $\mathbf{M_e}$. Finally, knowing the topology of the structural model, by rotating, expanding and assembling the local matrices of stiffness, $\mathbf{K_e}$, and mass, $\mathbf{M_e}$, the corresponding global matrices $\mathbf{K}$ and $\mathbf{M}$ are obtained (Bathe, 1982; Cheng, 2001; Zienkiewicz & Taylor, 2005). In our case, once given the required data input, all computations were automatically done by the adopted software. Moreover, the solution of the eigenvalue–eigenvector problem (9) was also obtained by the adopted finite element code. All models were left unconstrained in the 3D space, therefore, the rigid motions (i.e. eigenvectors corresponding to null eigenvalues) were disregarded from the solution.

Figure 2 shows the geometry of the three-dimensional finite element model implemented in LUSAS 15.1

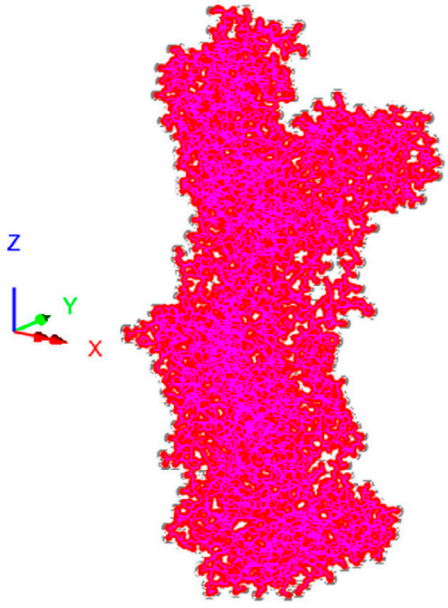

Figure 2. Geometry of the Na/K-ATPase finite element model.

(LUSAS, 2015). Starting from the spatial coordinates of the atoms composing the Na/K-ATPase crystal structure taken from the RCSB Protein Data Bank (http://www.rcsb.org/pdb) (access code: 2ZXE), a connectivity matrix was created in MATLAB (https://www.mathworks.com/products/matlab.html). According to a rather common conventional criterion, each atom was connected to all the others having a relative distance from it not greater than .2 nm. As a result, 10,351 connections were created among the 10,131 points (atoms) constituting the protein. The average connection (interatomic) distance is equal to .149 nm. A .dxf file containing the three-dimensional lattice was therefore created in MATLAB and imported in LUSAS to build the structural geometry. The average atom mass (total protein mass divided by number of atoms) is equal to 1.76×10^{-26} kg. Bond stiffness depends on of many factors, but firstly on the type of atoms involved; indicative values (in N m^{-1}) are the following (Ashby, Shercliff, & Cebon, 2014): 180 for C–C; 320 for C=C; 160 for C–N; 190 for C–O. C–C bonds are predominant in Na/K-ATPase, therefore a reasonable average value of bond stiffness is around 200 N m^{-1}. Since, in SI units, interatomic distances and atom masses are in the order of magnitude of 10^{-10} (m) and 10^{-26} (kg), respectively, we are dealing with powers of ten which are not appropriate for computer calculations; a numerical scaling was therefore introduced to build the model. Notice that such scaling is just an artifice introduced for making possible the computation and must not be intended as a physical scaling. According to the adopted numerical scaling listed in Table 1, the conversion between the real (subscript r) and the numerical model (subscript m) frequencies (in Hz) results to be the following:

$$f_r = f_m \times 10^{13}. \tag{12}$$

3D 3-node thin-beam finite elements were used in the model, with the default setting of 4 subdivisions per element; actually, the number of subdivisions has no influence on the solution regarding the axial elastic behaviour of the beam element (i.e. the equivalent linear spring simulating the interatomic bond), which is the only one of interest for the present analysis. The input parameters introduced in the analysis are listed in Table 2: a constant value of the point (atom) mass m_a = 1.76 kg was

Table 1. Scaling between real object and numerical model quantities.

Physical quantity	Scaling
Mass, M (kg)	Model = real × 10^{26}
Distance, L (m)	Model = real × 10^{10}
Stiffness, F L^{-1} (N m^{-1})	Model = real × 10^{0}

Table 2. Input data for numerical analysis.

Mass	Elastic properties of beams	Geometric properties of beams cross-section
Point (atom) mass, kg $m_a = 1.76$ Beam mass density, kg m^{-3} $\rho = 0$	Young's modulus, N m^{-2} $E = 3 \times 10^5$ Poisson's ratio, $v = .3$	Area, m^2 $A = 9.4 \times 10^{-4}$ Principal area moments of inertia, m^4 $I_1 = I_2 = 1 \times 10^6$ Torsion constant, m^4 $J = 1 \times 10^6$

used for all atoms; the beam mass density ρ was set equal to zero. Elastic constants were defined by Young's modulus $E = 3 \times 10^5$ N m^{-2} and Poisson's ratio $v = .3$. The beam cross-sectional area A was set equal to 9.4×10^{-4} m^2, the same for all beams. The principal area moments of inertia I_j and the torsion constant J (the same for all beams), were all set equal to 1×10^6 m^4. Note that, in this way, we have $EI_1/EA = EI_2/EA \approx 10^9$ and $GJ/EA \approx 10^8$, i.e. bending and torsion beam rigidities much greater than axial rigidity, according to what we pointed out before. Moreover, we remark that the selected values of Young's modulus and cross-sectional area have no physical basis: they were chosen such that the desired axial stiffness is obtained by Equation (11). For instance, using the area $A = 9.4 \times 10^{-4}$ m^2, Young's modulus $E = 3 \times 10^5$ N m^{-2}, and the average interatomic distance $l = 1.49$ m, Equation (11) yields an average axial (bond) stiffness k approximately equal to 190 N m^{-1}. Since, in the model, only the interatomic distance varies, and the stiffness k_i is inversely proportional to the beam length l_i, beams shorter than the average distance l will have a higher axial (bond) stiffness, whereas longer beams will result softer (lower bond stiffness).

The output of the numerical simulation was used to interpret previous experimental results obtained by the authors with Raman spectroscopy measurements conducted on lyophilized and rehydrated powder samples of adenosine 50′-triphosphatase (by Sigma-Aldrich; source: porcine cerebral cortex); see Lacidogna et al. (2017). Figure 3 shows the Raman spectrum of the lyophilized sample in the –500 to 500 cm^{-1} range: 1, 2, 3 indicate three low-frequency peaks at 27, 190, 300 cm^{-1} (i.e. .81, 5.70, 9.00 THz), respectively. To the best of the author's knowledge, such peaks are not yet assigned to any speci-

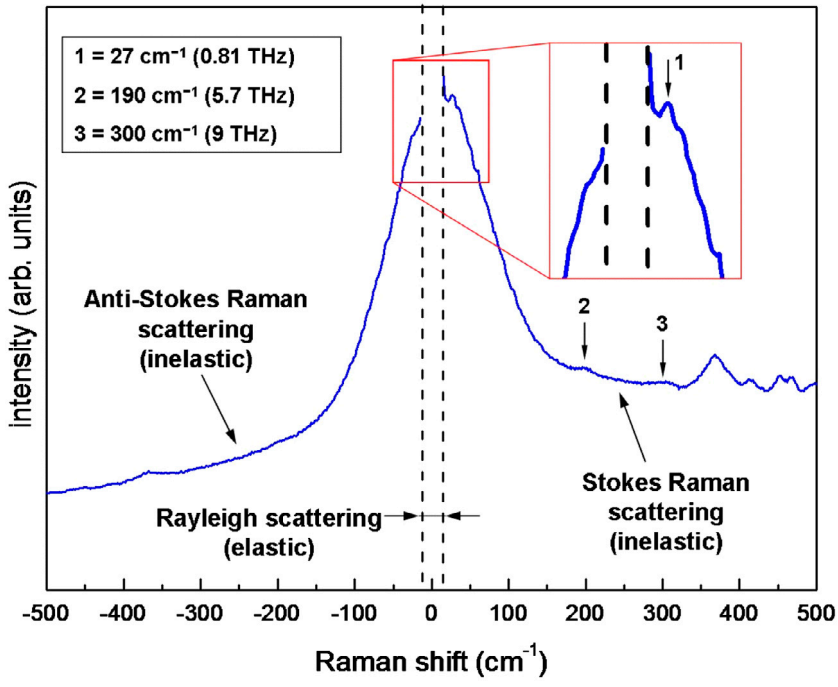

Figure 3. Raman spectrum of Na/K-ATPase (lyophilized powder sample) from previous experiments by the authors (see Lacidogna et al. (2017)) with indication of low-frequency peaks confirmed numerically (among others) in the present study.

fic vibration in the current literature of Na/K-ATPase; they are thus of great interest and are confirmed numerically, among others, in the present study. Among the abovementioned three peaks, the one at 27 cm^{-1} is of particular interest because it corresponds to a vibration below 1 THz.

3. Results

Figure 4 shows the mode shape found by the numerical model for a frequency close to the peak at 27 cm^{-1} in Figure 3. The experimental and numerical frequencies are respectively equal to .81 THz (27.0 cm^{-1}) and .82 THz (27.3 cm^{-1}). The figure shows a sequence of pictures taken from the same vibration cycle (deformations – i.e. eigenvectors – are defined but for a factor and are exaggerated for ease of visualization; they are to be intended as small-amplitude vibrations). This mode involves a large protein portion, in particular half of the protein end that extends inside the cell (top-left part in the figure), while all the rest of the protein is not involved.

Figure 5 shows the numerical mode shape corresponding to the frequency of 5.73 THz (191 cm^{-1}), i.e. the closest to the experimental peak at 5.70 THz (190 cm^{-1}) in Figure 3. In this case, the vibration involves the top-right part of the same protein end as before, i.e. the one extending inside the cell.

Figure 6 shows the numerical vibration mode at 9.06 THz (302 cm^{-1}), i.e. very close to the experimental frequency peak at 9.00 THz (300 cm^{-1}) in Figure 3. This mode corresponds to a vibration involving the entire bottom part of the protein, i.e. the one that extends outside the cell.

Figure 4. Numerical vibration mode at .82 THz (27.3 cm^{-1}) involving the top-left part of the protein.

Figure 5. Numerical vibration mode at 5.73 THz (190 cm^{-1}) involving the top-right part of the protein.

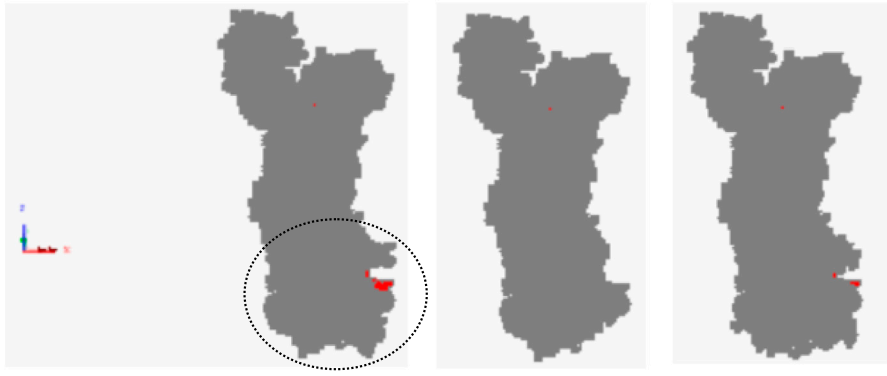

Figure 6. Numerical vibration mode at 9 THz (300 cm^{-1}) involving the bottom part of the protein.

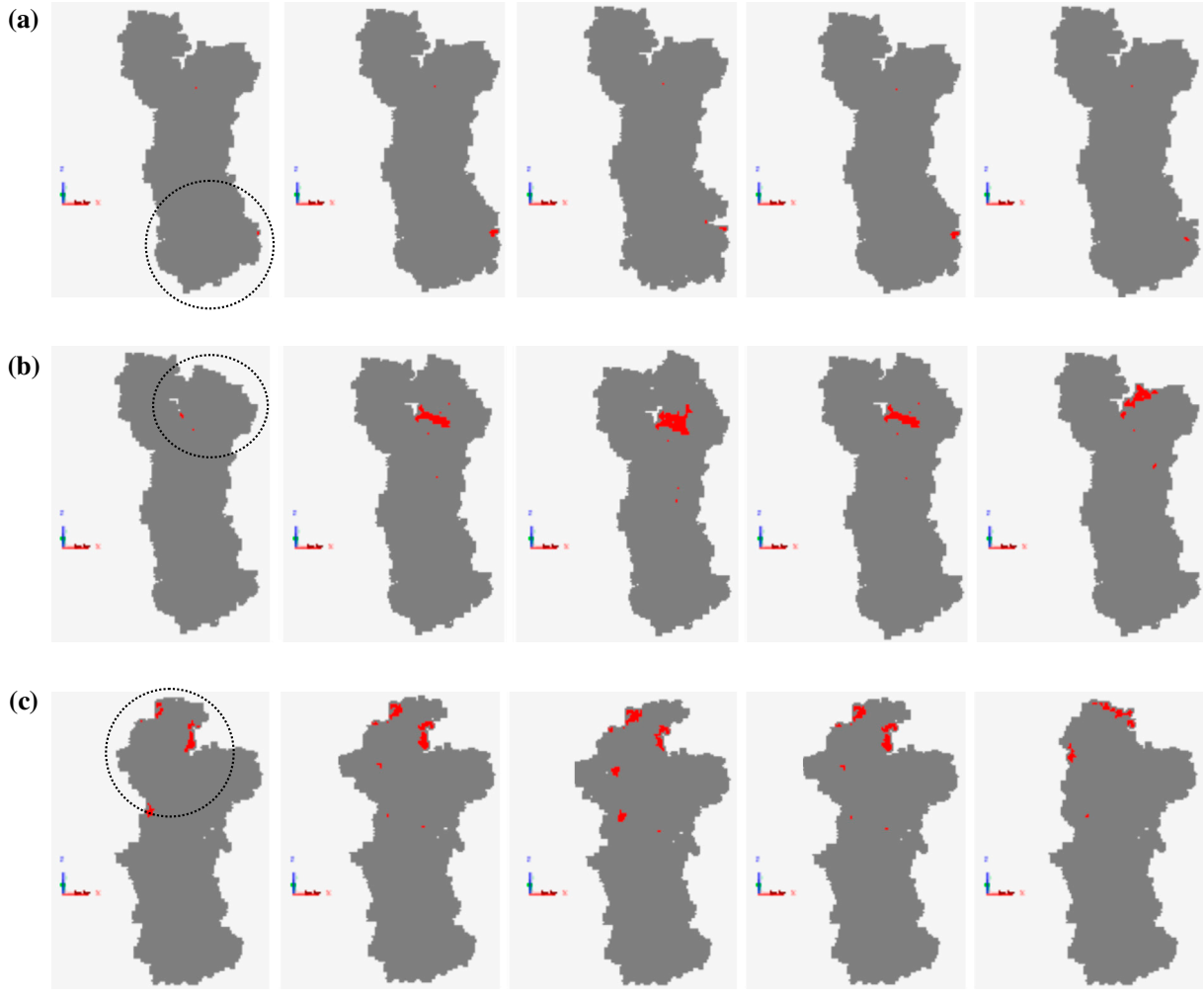

Figure 7. Other numerical vibration modes below 1 THz: (a) vibration mode at .51 THz (17 cm^{-1}) involving the bottom part; (b) vibration mode at .21 THz (7 cm^{-1}) involving the top-right part; and (c) vibration mode at .08 THz (2.7 cm^{-1}) involving the top-left part.

The numerical analysis was used to investigate other vibration modes at frequencies below the lowest one seen experimentally at .81 THz. Three numerical vibration modes similar to those of Figures 4–6, but at lower frequencies are shown in Figure 7. Figure 7(a)–(c) respectively show vibration modes at .51, .21 and .08 THz (i.e. 17, 7, and 2.7 cm^{-1}): the corresponding vibration modes involve the bottom part, the top-right part and the top-left part, respectively. However, for the last three frequencies we have no experimental counterparts at the moment.

The previous results were all obtained by a model where the entire protein was left unconstrained in the 3-D space, as we pointed out before. We checked that constraining the central part of the protein (i.e. the one inside the cell membrane and extending for about one third of the protein length) has no appreciable effects on the results presented previously. In fact, none of the modes shown above call into question the vibration of the central part of the protein.

4. Conclusions

In this paper, a numerical simulation was presented to investigate low-frequency vibration modes of Na/K-ATPase. An all-atom lattice model was built in the commercial finite element code LUSAS and a normal-mode analysis was run. Atoms were simulated by point masses (average atomic mass values were used), while interatomic bonds were replaced by beam elements simulating linear-elastic axial springs (bending and torsion deformations were prevented; average force constant of covalent bonds was used to set the beam axial stiffness). The simulation allowed associating a vibration mode shape to some low-frequency spectral peaks previously found experimentally by the authors via Raman spectroscopy (Lacidogna et al., 2017). Such frequency peaks appear to be new (i.e. not assigned to any specific vibration in the literature about Na/K-ATPase) and are of great interest because vibration modes near or below 1 THz are believed by the scientific community to be crucial in driving protein function. Some other vibration modes at frequencies even lower than those detected experimentally were also analysed in this study. The modes presented here involve vibration of the protein ends, therefore, they might in some way be related to the operating mechanism of the sodium-potassium pump.

Although further studies on the last issue are needed, nevertheless the two modal shapes related to the two intermediate natural frequencies of .82 and 5.73 THz seem to be the most interesting to investigate. As a matter of fact, they involve in the motion a more localized protein zone, which could facilitate folding of the ends and ionic migration through the cell membrane. In addition these frequencies, being close to the Debye frequencies of sodium and potassium, could induce resonance phenomena in atomic lattices of such chemical elements.

Disclosure statement

No potential conflict of interest was reported by the authors.

References

Ashby, M., Shercliff, H., & Cebon, D. (2014). *Materials: engineering, science, processing and design* (3rd ed.). Amsterdam: Butterworth-Heinemann.

Bathe, K. J. (1982). *Finite element procedures in engineering analysis*. Englewood Cliff, NJ: Prentice-Hall.

Bennett, W. S., & Huber, R. (1984). Structural and functional aspects of domain motions in proteins. *Critical Reviews in Biochemistry, 15*, 291–384.

Berendsen, H. J. C., & Hayward, S. (2000). Collective protein dynamics in relation to function. *Current Opinion in Structural Biology, 10*, 165–169.

Carpinteri, A. (1997). *Structural mechanics: A unified approach*. London: Chapman & Hall.

Carpinteri, A., Lacidogna, G., Piana, G., & Bassani, A. (2017). Terahertz mechanical vibrations in lysozyme: Raman spectroscopy vs modal analysis. *Journal of Molecular Structure, 1139*, 222–230.

Cheng, F. Y. (2001). *Matrix analysis of structural dynamics: Applications and earthquake engineering*. New York, NY: Marcel Dekker.

Clough, R. W., & Penzien, J. (1975). *Dynamics of structures*. New York, NY: McGraw-Hill.

Cui, Q., Li, G., Ma, J., & Karplus, M. (2004). A normal mode analysis of structural plasticity in the biomolecular motor F1-ATPase. *Journal of Molecular Biology, 340*, 345–372.

Feynman, R. P., Leighton, R. B., & Sands, M. (1964). *The Feynman lectures on physics*. Reading, MA: Addison-Wesley.

Gaillard, T., Dejaegere, A., & Stote, R. H. (2009). Dynamics of β3 integrin I-like and hybrid domains: Insight from simulations on the mechanism of transition between open and closed forms. *Proteins: Structure, Function, and Bioinformatics, 76*, 977–994.

Gerstein, M., & Krebs, W. A. (1998). A database of macromolecular motions. *Nucleic Acids Research, 26*, 4280–4290.

Gerstein, M., Lesk, A. M., & Chothia, C. (1994). Structural mechanisms for domain movements in proteins. *Biochemistry, 33*, 6739–6749.

Hayward, S., & Berendsen, H. J. C. (1998). Systematic analysis of domain motions in proteins from conformational change: New results on citrate synthase and T4 lysozyme. *Proteins: Structure, Function, and Genetics, 30*, 144–154.

Karplus, M., & Petsko, G. A. (1990). Molecular dynamics simulations in biology. *Nature, 347*, 631–639.

Lacidogna, G., Piana, G., Bassani, A., & Carpinteri, A. (2017). Raman spectroscopy of Na/K-ATPase with special focus on low-frequency vibrations. *Vibrational Spectroscopy, 92*, 298–301.

Liwo, A. (Ed.). (2013). *Computational methods to study the structure and dynamics of biomolecules and biomolecular processes: From bioinformatics to molecular quantum mechanics*. Berlin: Springer-Verlag.

Lucia, U. (2016). Electromagnetic waves and living cells: A kinetic thermodynamic approach. *Physica A: Statistical Mechanics and its Applications, 461*, 577–585.

Lucia, U., Grisolia, G., Ponzetto, A., & Silvagno, F. (2017). An engineering thermodynamic approach to select the electromagnetic wave effective on cell growth. *Journal of Theoretical Biology, 429*, 181–189.

Lucia, U., & Ponzetto, A. (2017). Some thermodynamic considerations on low frequency electromagnetic waves effects on cancer invasion and metastasis. *Physica A: Statistical Mechanics and its Applications, 467*, 289–295.

LUSAS. (2015). *User reference manual* (version 15.1), Kingston upon Thames: FEA Ltd.

McCammon, J. A. (1984). Protein dynamics. *Reports on Progress in Physics, 47*, 1–46.

McCammon, J. A., Gelin, B. R., & Karplus, M. (1976). The hinge-bending mode in lysozyme. *Nature, 262*, 325–326.

Morse, P. M. (1929). Diatomic molecules according to the wave mechanics. II. Vibrational levels. *Physical Review, 34*, 57–64.

Pauling, L. (1960). *The nature of the chemical bond* (3rd ed.). Ithaca, NY: Cornell University Press.

Rod, T. H., Radkiewicz, J. L., & Brooks, C. L. (2003). Correlated motion and the effect of distal mutations in dihydrofolate reductase. *Proceedings of the National Academy of Sciences, 100*, 6980–6985.

Tama, F., & Sanejouand, Y. H. (2001). Conformational change of proteins arising from normal mode calculations. *Protein Engineering, 14*, 1–6.

Tobi, D., & Bahar, I. (2005). Structural changes involved in protein binding correlate with intrinsic motions of proteins in the unbound state. *Proceedings of the National Academy of Sciences, 102*, 18908–18913.

Zienkiewicz, O. C., & Taylor, R. L. (2005). *The finite element method for solid and structural mechanics* (6th ed.). Amsterdam: Elsevier.